Journal of Photochemistry & Photobiology, A: Chemistry 468 (2025) 116458

Contents lists available at ScienceDirect

Journal of Photochemistry & Photobiology, A: Chemistry

journal homepage: www.elsevier.com/locate/jphotochem

New dye-sensitized solar cell (DSSC) based on $BiVO_4$ film and bixin natural dye

Antonio G.R. Costa [a], Luzia R. Santos [a], Paulo S.R. Meneses [b], Vicente G.F. Viana [c], Isolda Costa [d], Renato A. Antunes [e], Rejane M.P. Silva [a], Gustavo M. Gusmão [a], Geraldo E. Luz-Jr [a], Reginaldo S. Santos [a,*]

[a] GreenTec-PGQ-GERATEC-DQ- University of Piauí, João Cabral Street: N. 2231, P.O. Box 381, 64002-150 Teresina, PI, Brazil
[b] Department of Chemistry-PPGQ, Federal University of Piauí – UFPI, Campus Ministro Petrônio Portella, Ininga, Teresina 64049-550 PI, Brazil
[c] Postgraduate Program in Materials Engineering PPGEM, IFPI Central Campus, Teresina, Piauí, Brazil
[d] Institute for Energy and Nuclear Research – IPEN/CNEN, University City, São Paulo 05508-000 SP, Brazil
[e] Center for Engineering, Modeling, and Applied Social Sciences – Federal University of ABC/UFABC, Bangu, Santo André, 09210-580 SP, Brazil

ARTICLE INFO

Keywords:
$BiVO_4$/bixin solar cell
Renewable Energy
$LiClO_4$ additive

ABSTRACT

A new pathway to develop dye-sensitized solar cells is presented using bixin, lithium perchloride ($LiClO_4$) and bismuth vanadate ($BiVO_4$) formed electrochemically. Optical analysis showed the $BiVO_4$ film has a 2.37 eV band gap, suitable for visible sunlight. X-ray diffraction (XRD) revealed that the film is crystalline with a monoclinic phase. At the same time, morphological characterization carried out by Field Emission Scanning Electron Microscopy (FEG-SEM) showed that the film is porous and formed by particles measuring around 200 nm. Complete (photo)electrochemical studies were carried out for the photoanode, electrolyte, and bixin dye solution to evaluate the charge transfer energies of each solar cell component. $BiVO_4$/bixin film photovoltaic devices were fabricated using iodide/triiodide redox mediators and compared with dye-free $BiVO_4$ cells. Adding $LiClO_4$ to the electrolyte enhanced solar cell performance. Thus, the results presented in this paper indicate that solar cells formed by $BiVO_4$/bixin can be considered promising devices for converting solar energy into electrical current.

1. Introduction

Historically, humanity has depended on non-renewable energy sources such as oil, coal, and natural gas as civilization progressed [1–5]. However, the consumption of these energy sources, associated with the growth of the world population has generated environmental pollution problems that harm life on planet Earth [6–10]. Therefore, recent studies have investigated alternative energy sources that are more environmentally friendly [11,12].

The shift from polluting conventional energy sources to cleaner energy sources is known as the transition. The objective of changing from a polluting energy matrix to a cleaner energy source is to mitigate climate change and the problems it causes [12–15]. The cleanest energy sources include wind energy [16,17], hydropower [18,19], green hydrogen production [20,21], biomass [16,22], and photovoltaic energy. In this context, photovoltaic solar cells, also known as solarcells, can convert solar radiation directly into electrical current [17], which can be used to obtain hydrogen as a fuel source [23,24].

There are three generations of solar cell technologies. The first is crystalline silicon (Si) solar cells, with outstanding efficiency (about 30 per cent) and a life expectancy of up to 30 years. However, the most significant disadvantage of this technology is its high cost, which is attributed to the need to use high-purity Si [25]. Second-generation solar cells, also called thin-film cells, were developed to overcome this disadvantage. They are made of amorphous silicon, copper indium gallium selenide, cadmium telluride (CdTe), and copper tin sulfide [25,26]. Some authors reported that factors such as long-term stability, low efficiency, and toxicity are the main drawbacks of this cell type [25,26]. The third generation of photovoltaic cells includes quantum dot (QDSCs), perovskite (PSCs), organic (OSCs), and dye-sensitized solar cells (DSSCs). These new technologies offer several advantages, including a reported efficiency rate of up to 15 % [26,27].

Dye-sensitized solar cells (DSSCs), also called Grätzel solar cells [28,29], have the advantage of being simpler and cheaper to set up.

* Corresponding author.
E-mail address: rsantos.uespi@gmail.com (R.S. Santos).

https://doi.org/10.1016/j.jphotochem.2025.116458
Received 14 March 2025; Received in revised form 17 April 2025; Accepted 23 April 2025
Available online 27 April 2025

However, the cost-benefit ratio of these cells is only advantageous when more abundant raw materials are used in their manufacture. Thus, the type of sensitizing dye is a key material for DSSCs. Higher values of conversion efficiency of light into electric current are achieved with dyes that contain Ruthenium complexes [27,30,31]. However, DSSCs with these dyes are less attractive, considering that ruthenium dyes are expensive and harmful to the environment. In this scenario, recent research has explored alternative simpler, non-toxic, and biodegradable dye options for DSSCs [32,33]. This is why natural dyes are worth looking into. They can be extracted from different sources, such as fruits, flowers, leaves, and roots [32,33]. For instance, natural dyes norbixin and bixin as a sensitizer for DSSC devices were previously investigated by our research group [34]. The results showed that bixin was a good choice for making solar cells, which had an open circuit voltage (Voc) of 519 mV and a short circuit current (Jsc) of 0.195 mA [34].

Bixin is a natural reddish carotenoid pigment that can be found in annatto seeds. Thisconstitutes up to 80 % of the color of annatto seeds, commonly cultivated in tropical regions of the world, including some Brazilian states such as Amazônia, Pará, Maranhão, and Piauí. Bixin has also been used as a raw material for the food industry, in the production of cosmetics and pharmaceutical products [35–37]. As it is a widely used and cultivated natural dye, the use of bixin in photovoltaic devices can help make this technology cheaper.

The sensitization of TiO_2 and ZnO with natural dyes to play the role of photoanodes in DSSCs has already been demonstrated in a number of studies [26,38,39]. Both TiO_2 and ZnO are oxides that have a light absorption band in the ultraviolet region of the solar spectrum.

Therefore, the use of these oxides as electrodes for solar cells requires their modification with dyes. The dye molecules adsorbed on the oxide particles must be capable of absorbing radiation in the visible region of the solar spectrum and injecting electrons directly into the conduction band of the oxides. There are still very few studies on Grätzel-type solar cells, configured from colored oxide films. Recently, our research group proposed a dye-free photovoltaic device made up of colored electrodes acting as photoanode and photocathode, in a p-n type junction [40]. Similarly, other research has been carried out with colored semiconductor oxides, which include $CuWO_4$ [41], WO_3 [39], Cu_2O [40] and $BiVO_4$ [42] films.

$BiVO_4$ is an n-type semiconducting material with an estimated bandgap energy ranging from 2.3 to 2.5 eV [43]. The properties of this oxide in absorbing radiation in the visible region of the solar spectrum, its low cost, and low toxicity make it a potential material to act as a photoanode in solar cells [44]. $BiVO_4$ can be prepared by different methodologies, including hydrothermal method [45], sol–gel [46], and electrodeposition [47]. The electrochemical method can be considered the easiest way to prepare $BiVO_4$ films. Thus, using this methodology, the film is prepared directly on the conductive substrate, without requiring additional oxide deposition steps. Due to the excellent chemical stability of $BiVO_4$, this semiconductor has been used as a photocatalysis in studies on the photodegradation of organic pollutants in aqueous media [48], hydrogen water splitting [49,50], artificial CO_2 photosynthesis [51], supercapacitor systems [52] and solar cells [42,45,47]. However, based on the available literature, no studies still combine colored semiconductor film and natural dye to increase the efficiency of photovoltaic devices. Thus, in this work, we present studies on preparing a photovoltaic device configured with $BiVO_4$ film sensitized with the natural dye bixin. To support the results presented by the $BiVO_4$-bixin solar cell, a complete structural, optical, morphological, and photoelectrochemical characterization of the electrode is presented. For comparison purposes, the performance of the $BiVO_4$-bixin cell is compared with that of a TiO_2-bixin cell prepared under the same experimental conditions. The results achieved indicate that the solar cell investigated, formed by $BiVO_4$/bixin, has the potential for converting solar energy into electrical current.

2. Experimental method

2.1. Synthesis of the $BiVO_4$ film by electrodeposition method

$BiVO_4$ film was prepared using the electrodeposition method based on previously reported conditions [53,54]. Thin films were prepared on glass containing a conductive layer of tin oxide doped with fluorine (FTO-glass, from Sigma Aldrich, and resistivity of 7 Ω/sq). Before electrodeposition, the substrate was cut to a size of 1.0 × 2.5 cm^2, and -cleaned in an ultrasound bath in successive stages of neutral soap and water, deionized water, and acetone.

To prepare the $BiVO_4$ film by electrodeposition, initially, 100 mL of an aqueous precursor solution composed of 2.92 g of Bismuth III Nitrate ($Bi_5O(OH)_9(NO_3)_4$; Perfyl Tech®, 79 %) was prepared, 6 mL of Nitric Acid (HNO_3; Dinâmica®, 71 %), 20 mL of Monoethylene Glycol ($C_2H_6O_2$; Sigma-Aldrich®, 99.8 %) and deionized water. The electrodeposition process was carried out employing a Potentiostat/Galvanostat model PGSTAT302N from Metrohm® and NOVA 1.7 software. The analysis was performed in a single-chamber electrochemical unit equipped with a Teflon cover with three holes to accommodate the counter electrode (platinum wire), reference electrode (Ag/AgCl/KCl (3.0 mol L^{-1})), and working electrode (FTO-glass). During the electrodeposition process, eight chronoamperometric sweeps were applied, lasting 6 s each, under a constant potential of −1.85 V. Next, the formation of a dark-gray film was observed on the FTO-glass.

To convert the dark gray film into $BiVO_4$, 50 μL of a 0.1 mol L^{-1} solution of ammonium metavanadate (NH_4VO_3; Sigma-Aldrich®, 99 %) was dripped onto the electrodeposited metallic film. After that, the system was heat treated in an electric muffle furnace at 500 °C, heated at a rate of 2 °C min^{-1}, and maintained for 2 h. To remove the probable excess V_2O_5 formed during heat treatment, the film was immersed in 1.0 mol L^{-1} sodium hydroxide solution (NaOH; from Dynamic®, 98 %) for 3 min and then washed with deionized water.

2.2. Preparation of Pt film as counter electrode

The preparation of the platinum counter electrode (CE) was carried out based on previous studies by our research group [34]. Briefly, to prepare the CE, 10 μL of a 15 mmol/L solution of chloroplatinic acid hexahydrate (H_2PtCl_6 $6H_2O$; Sigma-Aldrich®, 37.50 %) was dripped onto the conductive face of the FTO-glass. Then, the conductive substrate was placed in an electric muffle furnace at 400 °C for 30 min. Subsequently, the CE was washed in an ultrasound bath in three steps: (i) mixing diluted neutral detergent and deionized water; (ii) only deionized water, and (iii) isopropanol. Before use, the CE was placed in an electric muffle furnace and heat-treated again, according to the previous configurations.

2.3. Preparation of the solution containing the bixin natural dye

The bixin natural dye was extracted following the methodology described by Fontinele et al [55]. The bixin solution was prepared from a mass of 0.0020 g of natural dye dissolved in 2 mL of ethanol (C_2H_6O; Dinâmica®, 99.5 %). This solution was maintained in ultrasonic bath treatment for one hour. Subsequently, the solution was transferred to a 5 mL volumetric flask, and the volume was adjusted with ethanol, resulting in a solution with a concentration of 1 × 10^{-3} mol L^{-1}.

2.4. Preparation of the electrolyte containing the I^-/I_3^- pair

The electrolyte was prepared by combining 0.32 g of iodine (I_2; Vetec, 99.8 %) and 0.36 g of ammonium iodide (NH_4I; Sigma-Aldrich®, 99 %) in a beaker. Thereafter, 15 mL of acetonitrile was added to the mixture and subjected to one hour of ultrasonic bath treatment. The mixture was then transferred to a 25 mL volumetric flask, and sufficient acetonitrile was added to form a solution with a concentration of 0.05

molL^{-1} of I_2 and 0.1 molL^{-1} of NH_4I. For the electrolyte solution with the additive, 0.0106 g of lithium perchlorate ($LiClO_4$; Sigma-Aldrich®, 95.0 %) was transferred to a 5 mL volumetric flask. Then, a 5 mL aliquot of the electrolyte was added, resulting in a solution with a concentration of 0.02 mol L^{-1} with the additive.

2.5. Characterization of structure, morphology and optics

The structural characterization of the films was carried out by X-ray diffraction(XRD), using an X-ray diffractometer, operating with Cu-Kα radiation (λ = 0.154 nm) at 40 kV at 30 mA, incident diffraction angle 2θ from 10° to 90° with 0.02°/min scan speed to assess the crystallinity and identify the phase of the sample. The Inorganic Crystal Structure Database (ICSD) was then used to compare the diffraction patterns. The optical properties of the material were investigated using UV–visible spectroscopy, this involved measuring the absorbance of the material using a Shimadzu® UV-2600 model spectrophotometer, with FTO-glass as reference. The morphology of the FTO|$BiVO_4$ sample was investigated with a field emission Scanning Electron Microscope (SEM-FEG, model VEGA3 LMU) VEGA3 from TESCAN, which operates with an acceleration voltage of 200 V to 30 kV. This equipment also allowed elemental analysis to be obtained using energy dispersive spectroscopy – EDS.

The elemental composition, chemical state, and electronic properties of the elements on the sample surface were obtained by X-ray photoelectron spectroscopy (XPS) using the K-alpha + model from Thermo Fisher Scientific®. The XPS instrument relies on an Al-Kα X-ray source and is calibrated concerning the C 1s peak at 284.43 eV.

2.6. Photoelectrochemical characterizations

Electrochemical measurements such as cyclic voltammetry (CV), linear sweep voltammetry (LSV), chronoamperometry, and chronopotentiometry, were conducted to investigate theperformance of the photoanode using a Potentiostat/Galvanostatmodel PGSTAT302N from Metrohm. Impedance Spectroscopy Measurements (EIS) were also performed using a Bipotentiostat/Galvanostat/Impedance Analyzer (EIS), Metrohm model μStat-i 400. These studies were conducted in the absence of or under polychromatic light irradiation, using a metal vapor lamp (HQI-NDL, 150 W, RX7S) adjusted to 100 mW cm^{-2}. In the photoelectrochemical studies, an aqueous solution of sodium sulfate (Na_2SO_4; Vetec, 99.0 %) 0.1 mol L^{-1} (pH 5.6) was used as the supporting electrolyte in a single-compartment electrochemical cell. The cell was configured with three electrodes, in which the $BiVO_4$ film was used as the working electrode, Ag/AgCl as the reference electrode and a Pt wire as the counter electrode.

Finally, $BiVO_4$-bixin solar cells were investigated by LSV under illumination at 100 mW cm^{-2} (AM 1.5). The linear scan rate was set at 2 mVs^{-1}, and the experimental data obtained from LSV curves were short-circuit photocurrent (J_{sc}), open-circuit voltage (V_{oc}), fill factor (FF), maximum power (P_{max}) and cell efficiency (η%).

3. Results and discussion

3.1. Structural characterization

Structural characterization of the FTO|$BiVO_4$ film was carried outby XRD analysis to evaluate the crystallinity and identify the type structure of the sample.

The diffractogram presented in Fig. 1 revealed diffraction signals in perfect agreement with ICSD card number 100604, for the monoclinic structure of $BiVO_4$ [42,56]. In the diffractogram it is possible to identify the signals attributed to reflection planes (002), (011), (112), (004), (200), (020), (1–21), (015), (123), (204), (220), (116), (312), (132), (224), (040) and (136)of $BiVO_4$ [57]. In addition, the diffraction peaks identified by asterisk (*) were attributed to the SnO_2, which forms theconductive layer (FTO) of the substrate (ICSD card number 409393).

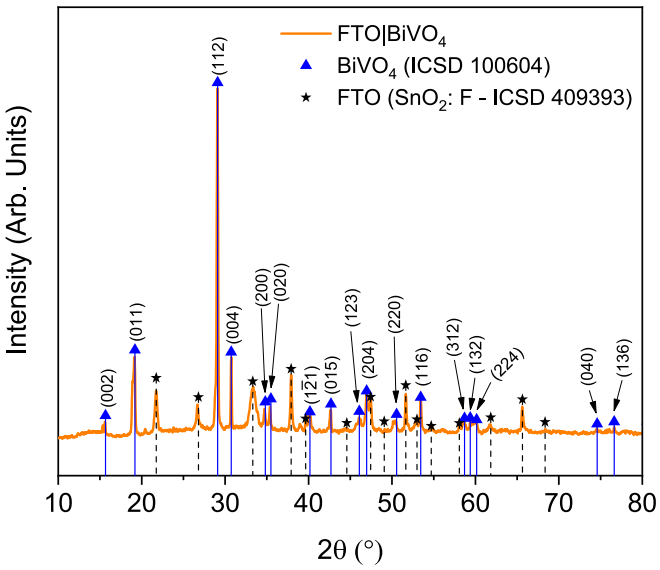

Fig. 1. XRD pattern for the FTO|$BiVO_4$ film calcined at 500 °C for 2 h. The vertical lines (|) indicate the positions and relative intensities found on the ICSD 100604 card for the monoclinic structure.

The results of the structural characterization showed that the applied synthesis process is well suited for the fabrication of $BiVO_4$ films on FTO-glass substrate.

3.2. Morphological and chemical composition studies

The images shown in Fig. 2 were obtained using Field Emission Scanning Electron Microscopy (FEG-SEM), which evaluated the morphology of the electrodeposited $BiVO_4$ film. The FEG-SEM image presented in Fig. 2a with a magnification of 15 k shows that the electrode is formed by several small grains (~200 nm) of undefined shape, agglomerated into larger particles, forming a porous film. The FEG-SEM image inset in Fig. 2a (magnification of 3 k) shows that the electrodeposition method forms a very regular film on the glass-FTO substrate. The porosity of the film can improve contact between $BiVO_4$ particles and the cell electrolyte, facilitating the charge transfer process [58]. The porous morphology may have been formed due to the release of volatiles and organic compounds such as monoethylene glycol during the heat treatment process, and the final treatment of the film with sodium hydroxide solution (see experimental section). Fig. 2b shows FEG-SEM image of the cross-section of the $BiVO_4$ film, where it is possible to observe that the non-regular and porous film has a thickness of approximately 2 μm.

The FTO|$BiVO_4$film composition was evaluated by energy-dispersive X-ray spectroscopy (EDS), which revealed a homogeneous distribution of bismuth (Bi), oxygen (O), and vanadium (V) atoms on the surface of the $BiVO_4$ sample. The table inserted in Fig. 3 presents the weight percentage (Wt%) of each element on the film surface, followed by the standard deviation (σ). Also, the atomic percentages detected by EDS were 15.66, 12.49, and 71.85 % for bismuth (Bi), vanadium (V), and oxygen (O), respectively. Theoretically, the atomic percentage ratio for [%O/(%Bi+%V)] for $BiVO_4$ should be 2.00 %. Based on the values estimated by EDS, the percentage was around 2.56 %. However, this higher value may be associated with the oxygen contributions from SnO_2, from the conducting layer.

Besides that, XPS investigation was developed to examine the chemical states of elements present in the film. XPS survey and high-resolution spectra depict signals for Bi 4f, V 2p and O 2 s registered in the BiVO4 sample. Fig. 4a displays XPS survey spectrum with peaks associated with Bi(4f) at 158.08 eV, O(1 s) at 529.08 eV, and V(2p) at 515.08 eV for the film, confirming the chemical composition of the

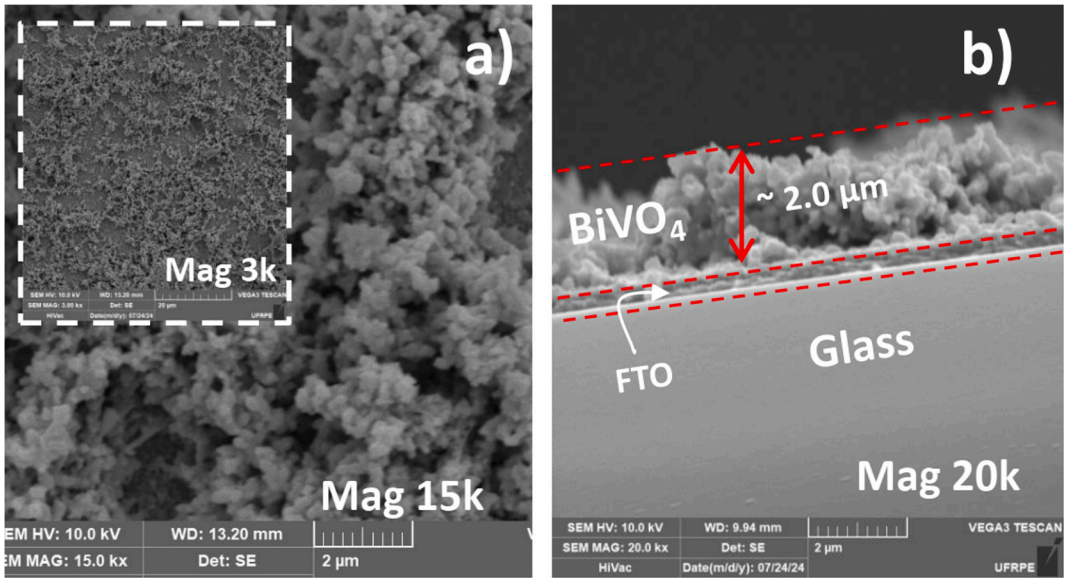

Fig. 2. a)FEG-SEM image of the surface and b) cross-sectionof FTO|$BiVO_4$ film prepared by electrodeposition method.

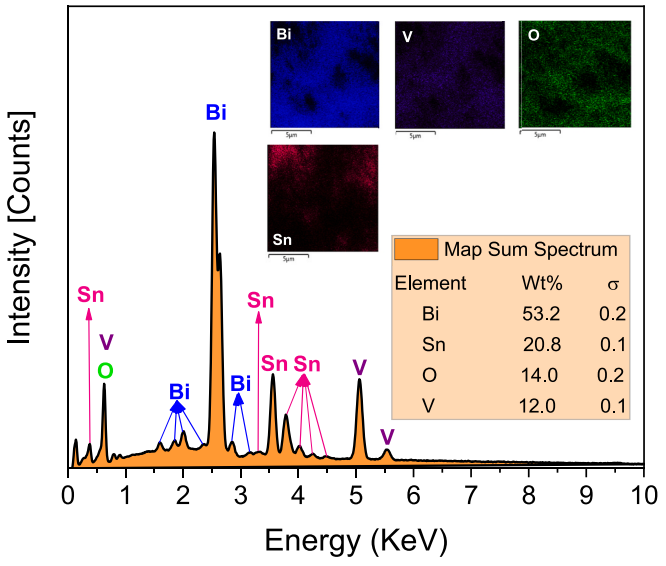

Fig. 3. EDS spectrum and mapping of the distribution of Bi, V, and O atoms on the surface of the $BiVO_4$ film.

sample registered early by EDS.

Fig. 4b shows the high-resolution spectrum for Bi $4f_{5/2}$ and $4f_{7/2}$, which exhibit two symmetric peaks with maximum binding energies (BE) values centered at 164.27 and 158.9 eV, respectively. These values are typical of Bi^{3+}, the valence state found in the $BiVO_4$ material [59,60]. The high-resolution spectrum shown in Fig. 4(c) corresponds to the BEattributed to electronic states of V^{5+} $2p_{3/2}$ and V^{5+} $2p_{1/2}$, which were located at516.57 and 524.05 eV, respectively. The BE value of 521.08 eV may be associated with vanadium bound to oxygen (V–O) [61–63].

The three Gaussian peaks in Fig. 4d correspond to the O 1 s peaks in the 529.6 to 531.5 eV region. These peaks were characteristic of oxygen in the B – O – V bond, oxygen vacancies, and oxygen of OH^- groups present on the surface of the material [64,65]. These hydroxyl groups may be associated with the basic solution used to remove excess vanadium oxide, probably formed during the heat treatment of the films.

3.3. Optical characterization

Fig. 5 shows the optical behavior of the unmodified FTO|$BiVO_4$ film with adsorbed natural bixin dye investigated using UV–Vis spectroscopy in absorbance mode. As can be seen in Fig. 5a, the $BiVO_4$ film exhibits light absorption in the visible region of the spectrum starting at approximately 550 nm. The increase in absorbance is due to electron transitions in the semiconductor. With the natural dye bixin, visible light absorption shifted to higher wavelengths, starting at 600 nm. Furthermore, the absorbance intensity was increased, indicating that the $BiVO_4$/bixin combination improves the harvest into the visible radiation. In TiO_2/dye solar cells, the mechanism of action of the dye for the operation of the device is presented as the injection of electrons from the dye directly into the CB of the TiO_2 [29,34]. In the case of the $BiVO_4$/bixin system, the electrons that reach the CB of the semiconductor must be the result of contributions from the oxide and the dye. Therefore, the colored semiconductor-bixin dye junction can work synergistically to convert radiation into electrical current.

Fig. 5(b) shows the optical band gap energy (E_{gap}) for the $BiVO_4$ film calculated by the Wood-Tauc function [66,67], as presented in Eq. (1). According to this methodology, the E_{gap} is obtained by extrapolating the linear part of the graph of $(\alpha h\nu)^{0.5}$ as a function of photon energy ($h\nu$). Considering an indirect transition, the E_{gap}value found was 2.37 eV, which is in agreement with the literature [42].

$$(\alpha h\nu)^n = C(h\nu - E_{gap}) \quad (1)$$

When not adsorbed on the $BiVO_4$ film particles, bixin presents a maximum absorbance at around 509 nm, as can be seen in Fig. S1 of the Supporting Information (SI). This absorption is in agreement with values previouslyreported [34,36]. Bixin's electronic transition is from highest occupied molecular orbital (HOMO) to lowest unoccupied molecular orbital (LUMO). This 509 nm wavelength of bixin, associated with electrochemical measurements, was used to find the energy difference between HOMO and LUMO of the dye, following the methodology previously investigated by our research group [34].

3.4. Electrochemical and photoelectrochemical analyses

3.4.1. Cyclic voltammograms of the electrolyte solution with $I^-|I_3^-$ and bixin natural dye

The electrolytes used in DSSCs are mainly composed of the redox pair $I^-|I_3^-$, with acetonitrile as the solvent. The redox couple may be used in

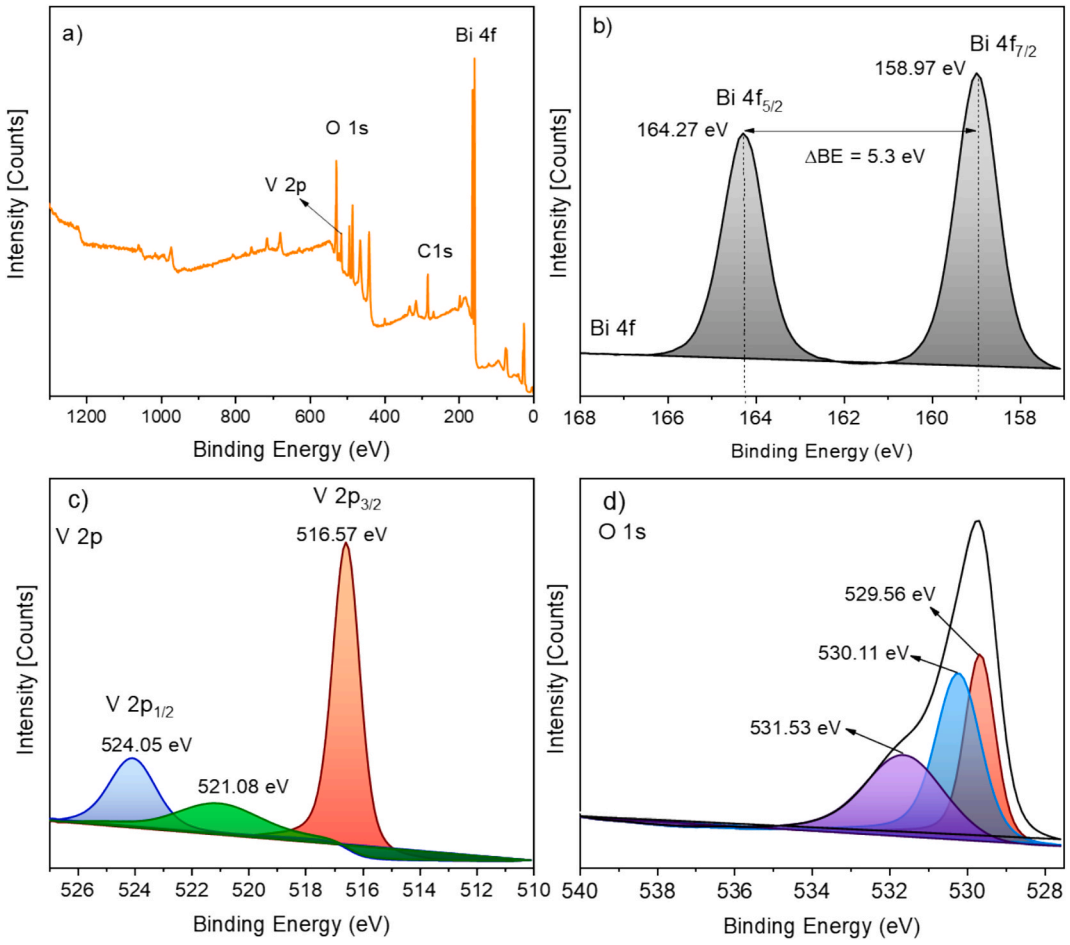

Fig. 4. XPS survey spectra (a) and high-resolution XPS spectrumof Bi 4f (b), V 2p (c), and O 1s (d).

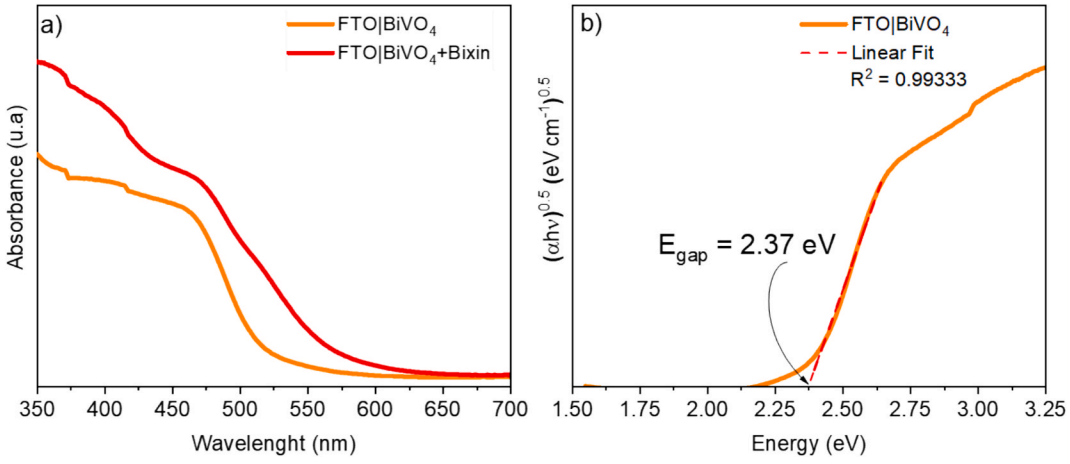

Fig. 5. UV–Vis curves in absorbance mode for a) FTO|$BiVO_4$ and FTO|$BiVO_4$ + bixin films and, b) calculated bandgap energy (E_{gap}) by the Wood-Tauc function for the FTO|$BiVO_4$ films assuming an indirect transition.

DSSCs to transfer electrons and regenerate photo-oxidized dyes [68,69]. Also, the use of acetonitrile may be linked to the high solubility of iodine and iodide salts in this solvent. Thus, iodide ions (I^-) play a significant role in the cell's efficiency, transiting between the photoanode and the cathode, undergoing oxidation–reduction, and contributing to the photocurrent density presented by the cell [70,71].

Fig. 6 shows Cyclic Voltammogram (CV) for $I^-|I_3^-$ electrolyte, and bixin natural dye in comparison with CV curve registered for the solvents. In Fig. 6a, no redox signal was observed for acetonitrile used as solvent. However, in the presence of the redox mediator, it is possible to observe an increase in anodic current that starts at around 0.50 V and a steady current at approximately 0.90 V (Ag/AgCl). In addition, the CV curve in the anodic and cathodic directions presents excellent hysteresis. The recorded potentials are associated with the redox balance in the $I_2 + I^- \rightleftharpoons I_3^-$ reaction. Potentials recorded with the Ag/AgCl reference electrode were converted to RHE and eV using equations 2 and 3

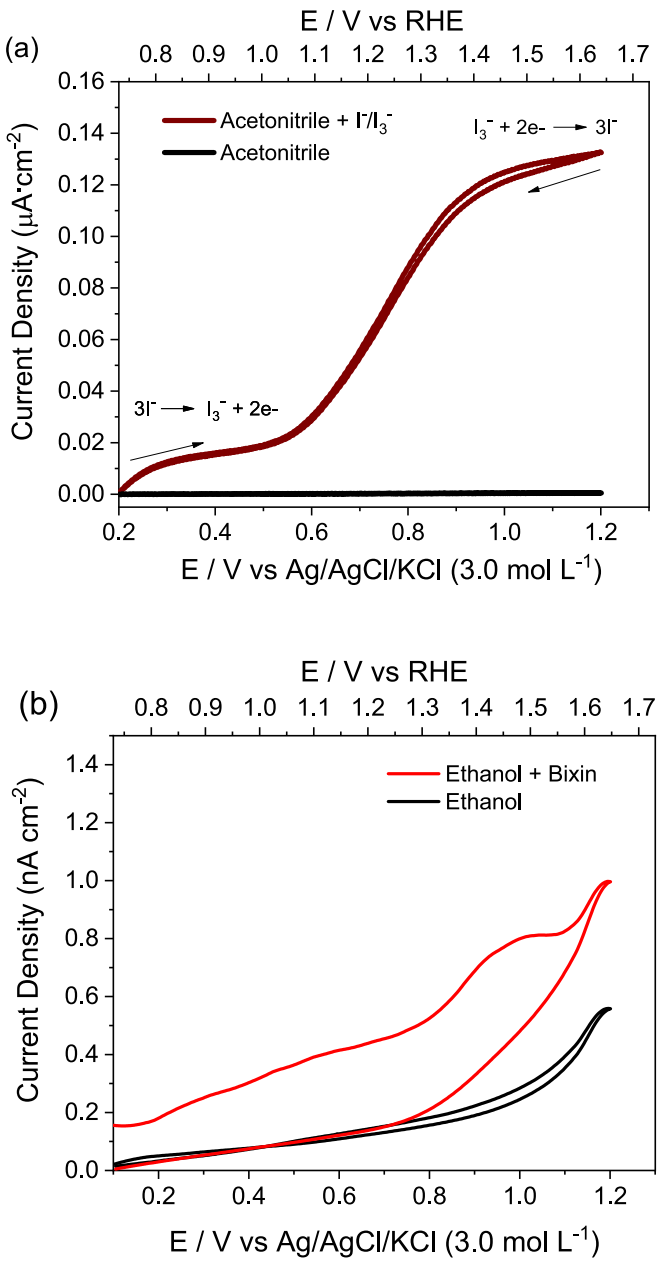

Fig. 6. CV curves for a) electrolyte solution to verify the $I^-|I_3^-$ redox pair, and b) solution containing the natural dye bixin obtained at a scan rate of 2 mV/s using a 10 μm diameter Pt microelectrode as the working electrode.

considering the electrolyte solution's pH, as presented in a previous study [72–74]. The redox potential values for the iodide-triiodide system were obtained in the range between −5.53 and −5.75 eV. The absence of diffusional behavior in the CV curve occurs because a microelectrode was used to study the redox potential of the electrolyte.

$$E\ (\text{vs, RHE}) = E\ (\text{vsAg/AgCl}) + 0.0591\ \text{V} \times \text{pH} + 0.199\ \text{V} \quad (2)$$

$$E(\text{eV}) = [-4.5\ \text{eV} - eE_{(\text{RHE})}] \quad (3)$$

Fig. 6b illustrates the CV curves for the ethanolic solution of bixin natural dye. The oxidation potential of bixin was observed atapproximately 1.0 V (Ag/AgCl). As presented previously, Eqs. 2 and 3 were used to convert this potential in RHE, which corresponds to −6.04 eV. Thus, considering the wavelength of maximum absorbance of bixin presented in Fig. S1 and the oxidation potential of the dye, it was possible to estimate the HOMO and LUMO of the molecule.

3.4.2. Photoelectrochemical characterization of FTO|$BiVO_4$ electrode

Photoelectrochemical measurements of semiconductor electrodes are important to evaluate the capability of the material to convert light into charges. The chronopotentiometry curve presented in Fig. S2 shows that $BiVO_4$ is an n-type semiconductor, with a negative photopotential variation (ΔE < zero). N-type semiconductors make excellent photoanodes in many light energy conversion systems. The $BiVO_4$ film was also subjected to electrochemical impedance spectroscopy (EIS) to evaluate the charge transfer behavior at the electrolyte–electrode interface. The Nyquist curves for the system in the dark condition compared to the irradiated system are shown in Fig. 7a. In both conditions, the electrode exhibits a single capacitive arc, which in higher frequency regions is associated with the charging of the electrical double layer and charge transfer processes. As observed in the FEG-SEM images in Fig. 2, the $BiVO_4$ electrode is porous and this porosity facilitates contact at the electrode/electrolyte interface, thus improving charge transfer. Under illumination conditions, it was possible to observe the lowest impedance values and a smaller capacitive arc, observed by the smaller semicircle diameter (orange curve), indicating that the electrode presented a lower resistance to charge transfer when compared to the non-irradiated condition (black curve).

Fig. 7b shows the Linear Sweep Voltammogram (LSV) for the FTO|$BiVO_4$ electrode, registered in a potential interval of −0.1 to 1.2 V, with interruption of the irradiation every 10 s and scan rate of 2 mV s^{-1}. In the dark condition, the $BiVO_4$ film presents almost zero current. On the other hand, under polychromatic light illumination conditions, the photoelectrode shows a gradual increase in photocurrent, reaching approximately 75 μA cm^{-2} of anodic current at 0.7 V (Ag/AgCl). When irradiated, electrons are promoted from CV to CB of $BiVO_4$. In the dark condition, electrons return to VB of the material and the recorded current is almost zero again. From Impedance analyzer, it is possible to estimate the flat band potential (E_{fb}) for $BiVO_4$, using the Mott-Schottky (MS)described by Eq. (4).

$$\frac{1}{C_{sc}^2} = \frac{2}{\varepsilon_0 \varepsilon_r A^2 e N_D}\left(E - E_{fb} - \frac{K_B T}{e}\right) \quad (4)$$

where C_{SC} semiconductor capacitance; ε_0 and ε_r refer to vacuum permittivity and relative permittivity, respectively; A is the surface area; e is electron charge; N_D is the majority carrier density; E is applied potential; K_B is the Boltzmann's constant and, T the temperature [75]. Fig. 7c shows the value of −0.045 V (vs Ag/AgCl) for E_{fb} of BiVO4. In n-type semiconductors, the Fermi potential (E_F) is close to the CB of the material. Thus, considering the band edge potential (E_{CB}) ~ E_{fb}, it was possible to estimate the E_{CB} of $BiVO_4$, according to Eq. (4), and following metrology presented in previous studies by our research group [76,77]. Thus, the E_{CB} was estimated at −0.045 V, which corresponds to −4.98 eV.

Additional photoelectrochemical studies also revealed that even under biaspotential, $BiVO_4$ films show electron-hole charge recombination. Fig. 3Sa shows the chronoamperometric curve recorded for the system polarized at 0.70 V (Ag/AgCl) in light–dark conditions. In the dark, it can be observed that the current density is nearly zero, as registered in CV curves. However, immediately after light illumination, ananodic photocurrent peak is observed, which can be attributed to the separation and accumulation of charges in the CB of the semiconductor. It is then evident that the photocurrent reduces exponentially until it reaches a stationary state. This reduction in photocurrent can be attributed to the recombination kinetics of the photogenerated charges. Based on the methodology previously presented by our research group [72,76,77]. The recombination time of the electron-hole pair was estimated at 27 s. Another important observation is that the photocurrent intensity remains practically unchanged throughout the repeated light–dark cycles, suggesting a good resilience of $BiVO_4$ to photocorrosion.

From the E_{CB} and E_{gap} values (presented in Fig. 2b) it was possible to

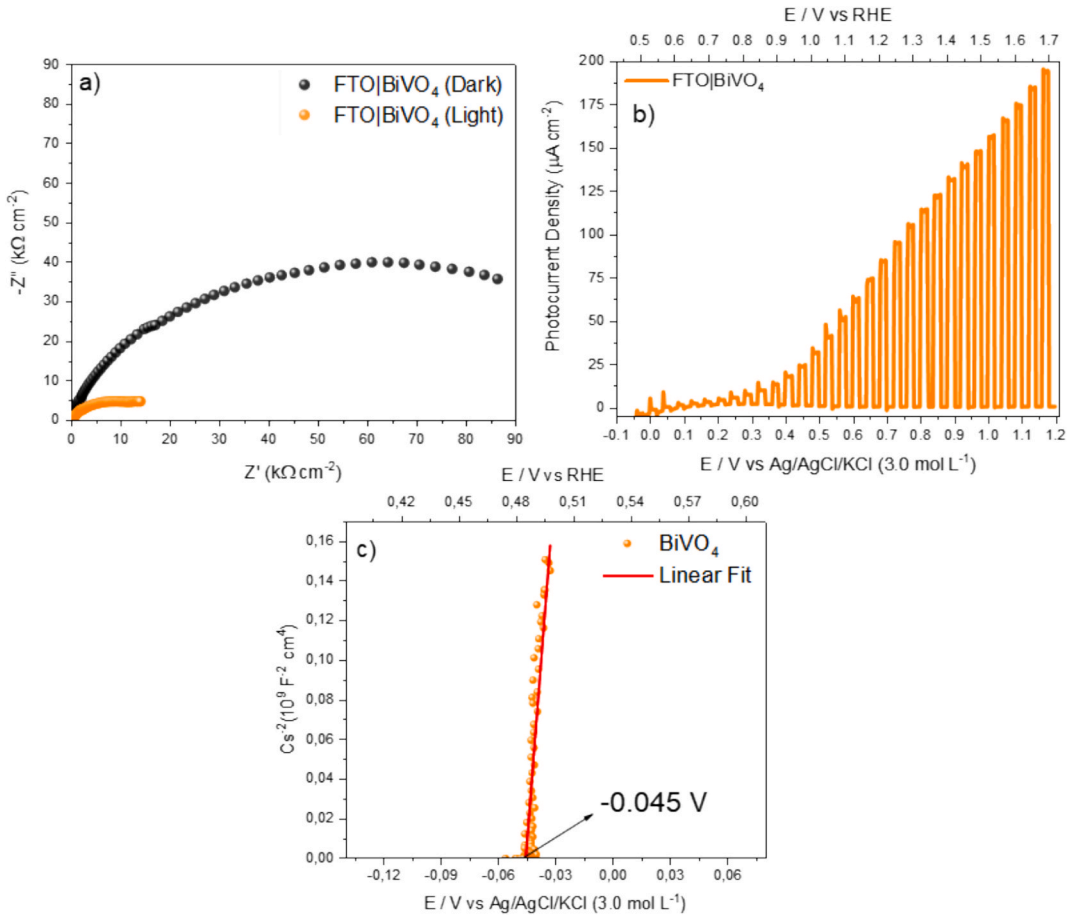

Fig. 7. a) Nyquist diagrams for the FTO|$BiVO_4$ electrode obtained in the absence of and under polychromatic irradiation, b)LSV curve for the FTO|$BiVO_4$electrode under interrupted polychromatic light irradiation every 10 s and scan rate 2 mVs^{-1}, obtained in 0.1 $molL^{-1}$ Na_2SO_4aqueous solution as support electrolyte and c) Mott-Schottky plots for the FTO|$BiVO_4$ electrode under dark conditions.

estimate the value of the valence band edge potential (E_{VB}). Considering the E_{CB}, E_{gap}, and E_{VB} values, it was possible to construct the diagram displayed in Fig. 8. According to the diagram, the energy values of the electrolyte, dye, and semiconductor are suitable for the application of the system in solar energy conversion, since the solar cell allows an adequate transfer of charges.

As illustrated in the diagram shown in Fig. 8, when the solar cell based on $BiVO_4$/bixin is irradiated, the bixin dye has electrons excited

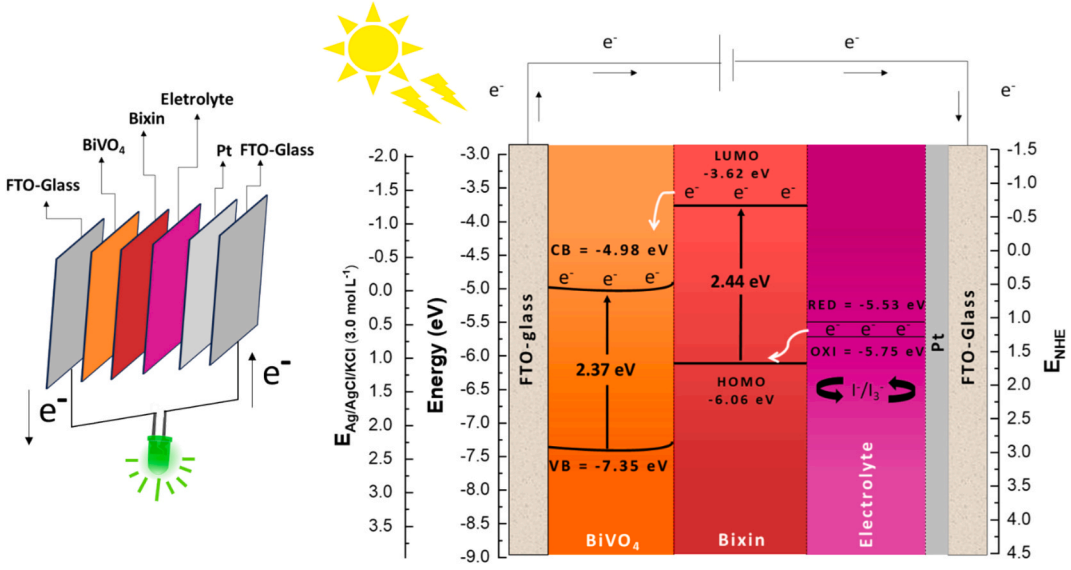

Fig. 8. Diagram illustratingthe energy levels of the constituents of the solar cell, with the positions of the CB and VB of the FTO|$BiVO_4$ film electrode; the HOMO and LUMO of the dye, and the redox level of the electrolyte constituting the solar cell.

from HOMO to LUMO. As $BiVO_4$ displays an E_{CB} positioned above that of the LUMO of the bixin dye, the transfer of electrons excited in the dye to the CB of the semiconductor occurs. To regenerate the oxidized dye, the redox potential of the electrolyte must exceed the HOMO. As $BiVO_4$ is colored, the electrons that reach the CB of the material may also have been injected from the VB of the semiconductor. As observed for the dye, the electrolyte has a redox potential above the E_{VB} and can regenerate the lost charge. Thus, based on the estimated potentials, it is possible to propose that the mechanism that explains the photocurrent in the $BiVO_4$/bixin solar cell arises when, under irradiation, electrons are excited from the HOMO to the LUMO of the dye, being subsequently injected into the $BiVO_4$ BC. Thus, these electrons reach the external circuit and arrive at the platinum counter electrode. During this process, the electrolyte has adequate potential to restore the dye or the gap left in the VB of the semiconductor.

3.5. Photoelectrochemical characterizations of $BiVO_4$/bixin solar cells

Fig. 9 shows the photoelectrochemical characterization of solar cells prepared from the FTO|$BiVO_4$ film modified or not with the natural current bixin. Photocurrent versus voltage measurements were recorded under a polychromatic light source adjusted to 100 mW cm^{-2} (1.5AM). A $BiVO_4$ solar cell without bixin had a Voc of 302 mV and a Jsc of 0.315 mA cm^{-2}. Similar efficiency (η %) was registered by Daemi et al [78] for dye-free $BiVO_4$solar cell prepared with liquid electrolyte. In our study, whenthe $BiVO_4$ film was modified with bixin, the solar cell showed higher V_{oc} and J_{sc} values. This result corroborates the UV–Vis data that indicated the superior capacity of the $BiVO_4$/bixin photoanode to absorb polychromatic radiation.

As discussed earlier, from the energy level diagram, the redox level of the electrolyte is suitable for the regeneration of the dye, which in turn is capable of injecting electrons into the CB of $BiVO_4$. The $BiVO_4$/bixin solar cell was also evaluated in the presence of lithium perchlorate ($LiClO_4$) as an electrolyte additive. Fig. S4 shows CV curve of the electrolyte containing $LiClO_4$, with a higher current value, compared to the iodide/triiodide systemwithout the presence of the additive. As seen in Fig. 9, the $LiClO_4$ contributed to increasing the J_{sc} and V_{oc} of the solar cell. As can be seen in Fig. S4, the organic solvent acetonitrile used in the preparation of the electrolytic solution does not present a redox signal in the investigated potential region. In addition, the acetonitrile and $LiClO_4$ system also does not present a current signal in the cyclic voltammogram shown in Fig. 4S. This result suggests that the additive functions as an electrolytic salt, increasing the ionic conductivity of the electrolyte and decreasing the charge transfer resistance in the solar cell.

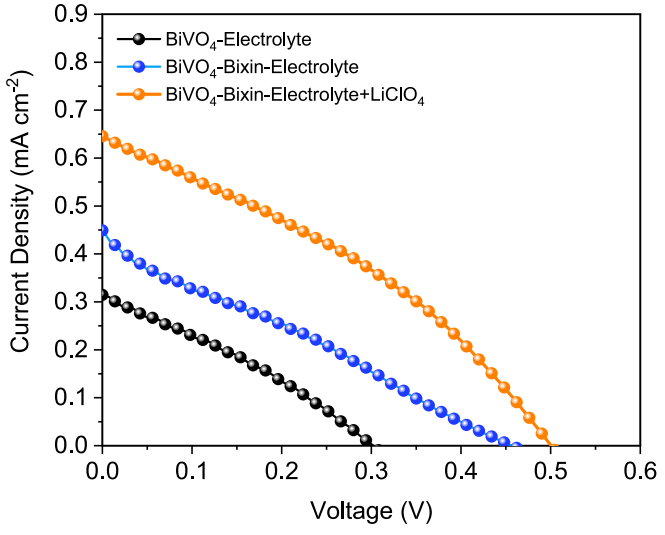

Fig. 9. $J_{sc} \times V_{oc}$ curves for cells not sensitized (black curve) and sensitized with the Bixin dye in the presence (orange curve) and absence (blue curve) of the additive ($LiClO_4$).

Table 1 summarizes the results of open circuit voltage (V_{oc}), short-circuit current density (J_{sc}), maximum power (P_{max}), fill factor (FF), and efficiency (η) of the solar cells presented in these studies. It is possible to note that the presence of $LiClO_4$ in the electrolyte increased the overall efficiency of the photovoltaic device by approximately 1.75 times, while the presence of the dye contributed to an increase of approximately 1.89 times. The highest efficiency observed was 1.11 % for solar cells made of $BiVO_4$/bixin film and $LiClO_4$ as an additive. In comparison to the dye-free solar cell, the overall efficiency of the best device was approximately 3.96 times.

The theoretical capacity of a photovoltaic cell to convert light to current can be monitored through several parameters, which include fill factor (FF), short-circuit current density (J_{sc}) and open-circuit voltage (V_{oc}). In a J versus V curve, the maximum power point (P_{max}) is obtained at values of J_{max} and V_{max}. FF is a parameter that relates P_{max}, J_{sc} and V_{oc}, according to Eq. (5):

$$FF = \frac{P_{max}}{J_{sc} \times V_{oc}} = \frac{J_{max} \times V_{max}}{J_{sc} \times V_{oc}} \quad (5)$$

In principle, the highest value obtained for FF is unity, when the values of J_{sc} and V_{oc} are equal to J_{max} and V_{max}, respectively. The fill factor (FF) of a solar cell is a measure of how rectangular its current–voltage (J-V) curve is. A higher FF indicates a more rectangular curve, while a lower FF indicates a flatter curve. Thus, a rectangular J-V curve indicates that the value of J_{sc} remains almost constant even under reverse bias conditions of the photovoltaic device.

The efficiency (η%) of conversion of incident light power (P_{in}) into photocurrent is another important parameter to evaluate the quality of a solar cell. This efficiency can be calculated according to Eq. (6):

$$\eta(\%) = \frac{P_{max}}{P_{in}} \times 100 = \frac{J_{max} \times V_{max}}{P_{in}} \times 100 = \frac{J_{sc} \times V_{oc} \times FF}{P_{in}} \times 100 \quad (6)$$

The parameters obtained for all investigated devices and presented in Table 1 indicate that the cell prepared with $BiVO_4$, modified with bixin and having $LiClO_4$ as an additive is the best photovoltaic device.

4. Conclusion

$BiVO_4$ films were successfully prepared from the electrochemical deposition of metallic bismuth followed by heat treatment in the presence of a vanadium source. The films presented excellent adhesion to the FTO-glass substrate. The structural characterization of the sample showed that the material has a monoclinic phase, while FEG-SEM images revealed the presence of clusters of particles measuring around 200 nm. Photoelectrochemical measurements demonstrated that $BiVO_4$ forms an n-type semiconductor electrode with a photocurrent density of approximately 75 μA cm^{-2}, at 0.7 V (vs Ag/AgCl). The estimated value of the optical E_{gap} for the material is in agreement with values reported in the literature and indicates that the material absorbs light in the visible region of the solar spectrum. This light absorption region and intensity were enlarged for the $BiVO_4$/bixin system, which is an ideal condition for good DSSC performance. The energy level diagram obtained for all components of the solar cell indicated that the charge

Table 1
DSSC parameters (J_{sc}, V_{oc}, FF, P_{max}, and η(%)) extracted from the graph shown in Fig. 9.

Parameters	FTO|$BiVO_4$-Electrolyte	FTO|$BiVO_4$/bixin-Electrolyte	FTO|$BiVO_4$/bixin-Electrolyte + $LiClO_4$
V_{oc} (mV)	302	454	500
J_{sc}(mA)	0.315	0.449	0.646
FF	0.297	0.260	0.344
P_{max} (mW)	28.22	52.65	111
η (%)	0.28	0.53	1.11

transfer kinetics is favored in the solar cell formed with the $BiVO_4$/bixin electrode, having the iodide/triiodide redox pair in the electrolyte. The diagram also showed that the bixin dye is suitable for injecting electrons into the CB of the semiconductor. The studies presented also demonstrated that the incorporation of $LiClO_4$ as an additive increased the photocurrent density of solar cells. Thus, the results indicate that the $BiVO_4$ film sensitized with bixin dye can be considered a promising material for use as a photoanode in a photovoltaic device.

CRediT authorship contribution statement

Antonio G.R. Costa: Writing – original draft, Validation, Methodology, Investigation, Data curation, Conceptualization. **Luzia R. Santos:** Methodology, Formal analysis, Conceptualization. **Paulo S.R. Meneses:** Investigation, Formal analysis, Data curation. **Vicente G.F. Viana:** Investigation, Data curation. **Isolda Costa:** Investigation, Data curation. **Renato A. Antunes:** Investigation, Formal analysis, Data curation. **Rejane M.P. Silva:** Writing – review & editing, Resources, Methodology, Investigation. **Gustavo M. Gusmão:** Investigation, Formal analysis, Data curation. **Geraldo E. Luz-Jr:** Writing – review & editing, Methodology, Funding acquisition, Conceptualization. **Reginaldo S. Santos:** Writing – review & editing, Supervision, Resources, Project administration, Methodology, Funding acquisition, Conceptualization.

Declaration of competing interest

The authors declare that they have no known competing financial interests or personal relationships that could have appeared to influence the work reported in this paper.

Acknowledgments

The authors would like to thank the research funding agencies FAPEPI, CAPES (Process: 88887.931740/2024-00, 88881.691127/2022-01 and88887.800874/2023-00), and CNPq (Process number 310720/2023-0) for scholarships granted to research participants and other financial support.

Appendix A. Supplementary data

Supplementary data to this article can be found online at https://doi.org/10.1016/j.jphotochem.2025.116458.

Data availability

No data was used for the research described in the article.

References

[1] F. Rehman, I.H. Syed, S. Khanam, S. Ijaz, H. Mehmood, M. Zubair, Y. Massoud, M. Q. Mehmood, Fourth-generation solar cells: a review, Energy Adv. 2 (2023) 1239–1262, https://doi.org/10.1039/D3YA00179B.
[2] S. Dixit, Solar technologies and their implementations: A review, Mater. Today Proc. 28 (2020) 2137–2148, https://doi.org/10.1016/j.matpr.2020.04.134.
[3] P.M. de Souza, C.E.S. de Andrade, C.I. de Campos, Evaluation of the use of different urban freight transport vehicles in the last mile, from the perspectives of technology and sustainability, RECIMA21 – Multidisciplinary Sci. J. (5) (2024) e514854, https://doi.org/10.47820/recima21.v5i2.4854.
[4] A. De Brito Maier, A. Cristina Santos, F. Batista Araújo, G. Eliza Gama Vieira, Biofuels and the mitigation of GEE emissions: a question of sustainability, desafios, Interdiscip. J. Federal Univ. Tocantins 8 (2022) 161–173, https://doi.org/10.20873/uftv8-11190.
[5] F.F.S. Marquesan, J.B. Silva, The Socioeconomic Appeal and Entrepreneurial Action in the Structuring Process of Productive Configurations Linked to Bioenergy in Brazil, Develop. Question 19 (2021) 22–36, https://doi.org/10.21527/2237-6453.2021.55.10185.
[6] M. Carvalho, J.N. de Figueiredo, G.C.D. Cavalcanti, R.S. Freire, L. Machado, R. Abrahão, Environmental education through a carbon footprint quantification app, Res., Soc. Develop. 10 (2021) e0710111058, https://doi.org/10.33448/rsd-v10i1.11058.
[7] N. Abas, A. Kalair, N. Khan, Review of fossil fuels and future energy technologies, Futures 69 (2015) 31–49, https://doi.org/10.1016/j.futures.2015.03.003.
[8] W. Fulkerson, R.R. Judkins, M.K. Sanghvi, Energy from Fossil Fuels, Sci. Am. 263 (1990) 128–135. http://www.jstor.org/stable/24996937.
[9] R.A. Barreto, Fossil fuels, alternative energy and economic growth, Econ. Model. 75 (2018) 196–220, https://doi.org/10.1016/j.econmod.2018.06.019.
[10] F. Barbir, T.N. Veziroğlu, H.J. Plass, Environmental damage due to fossil fuels use, Int. J. Hydrogen Energy 15 (1990) 739–749, https://doi.org/10.1016/0360-3199(90)90005-J.
[11] P. Li, Z. Lin, H. Du, T. Feng, J. Zuo, Do environmental taxes reduce air pollution? Evidence from Fossil-Fuel Power Plants in China, J. Environ. Manage. 295 (2021) 113112, https://doi.org/10.1016/j.jenvman.2021.113112.
[12] M.W. Zafar, M. Shahbaz, A. Sinha, T. Sengupta, Q. Qin, How renewable energy consumption contribute to environmental quality? The Role of Education in OECD Countries, J. Clean Prod. 268 (2020) 122149, https://doi.org/10.1016/j.jclepro.2020.122149.
[13] Z. Wu, X. Fan, B. Zhu, J. Xia, L. Zhang, P. Wang, Do government subsidies improve innovation investment for new energy firms: A quasi-natural experiment of China's listed companies, Technol. Forecast Soc. Change 175 (2022) 121418, https://doi.org/10.1016/j.techfore.2021.121418.
[14] A.G. Olabi, M.A. Abdelkareem, Renewable energy and climate change, Renew. Sustain. Energy Rev. 158 (2022) 112111, https://doi.org/10.1016/j.rser.2022.112111.
[15] J.L. Holechek, H.M.E. Geli, M.N. Sawalhah, R. Valdez, A Global Assessment: Can Renewable Energy Replace Fossil Fuels by 2050? Sustainability (Switzerland) 14 (2022) https://doi.org/10.3390/su14084792.
[16] L. Amjith, B. Bavanish, A review on biomass and wind as renewable energy for sustainable environment, Chemosphere 293 (2022) 133579, https://doi.org/10.1016/j.chemosphere.2022.133579.
[17] M. Rezaei, A. Mostafaeipour, N. Jafari, N. Naghdi-Khozani, A. Moftakharzadeh, Wind and solar energy utilization for seawater desalination and hydrogen production in the coastal areas of southern Iran, J. Eng., Des. Technol. 18 (2020) 1951–1969, https://doi.org/10.1108/JEDT-06-2019-0154.
[18] Y. Zhang, H. Ma, S. Zhao, Assessment of hydropower sustainability: Review and modeling, J. Clean. Prod. 321 (2021) 128898, https://doi.org/10.1016/j.jclepro.2021.128898.
[19] A. Wasti, P. Ray, S. Wi, C. Folch, M. Ubierna, P. Karki, Climate change and the hydropower sector: A global review, WIREs Clim. Change 13 (2022), https://doi.org/10.1002/wcc.757.
[20] A.M. Oliveira, R.R. Beswick, Y. Yan, A green hydrogen economy for a renewable energy society, Curr. Opin. Chem. Eng. 33 (2021) 100701, https://doi.org/10.1016/j.coche.2021.100701.
[21] S. Shiva Kumar, H. Lim, An overview of water electrolysis technologies for green hydrogen production, Energy Reports 8 (2022) 13793–13813, https://doi.org/10.1016/j.egyr.2022.10.127.
[22] N. Tukenmez, M. Koc, M. Ozturk, A novel combined biomass and solar energy conversion-based multigeneration system with hydrogen and ammonia generation, Int. J. Hydrogen Energy 46 (2021) 16319–16343, https://doi.org/10.1016/j.ijhydene.2021.02.215.
[23] J. Zhang, B. Ling, Y. He, Y. Zhu, Z. Wang, Life cycle assessment of three types of hydrogen production methods using solar energy, Int. J. Hydrogen Energy 47 (2022) 14158–14168, https://doi.org/10.1016/j.ijhydene.2022.02.150.
[24] G.K. Karayel, N. Javani, I. Dincer, Green hydrogen production potential for Turkey with solar energy, Int. J. Hydrogen Energy 47 (2022) 19354–19364, https://doi.org/10.1016/j.ijhydene.2021.10.240.
[25] M. Gul, Y. Kotak, T. Muneer, Review on recent trend of solar photovoltaic technology, Energy Explor. Exploit. 34 (2016) 485–526, https://doi.org/10.1177/0144598716650552.
[26] M.V. Dambhare, B. Butey, S.V. Moharil, Solar photovoltaic technology: A review of different types of solar cells and its future trends, J. Phys. Conf. Ser. 1913 (2021) 012053, https://doi.org/10.1088/1742-6596/1913/1/012053.
[27] N. Tomar, A. Agrawal, V.S. Dhaka, P.K. Surolia, Ruthenium complexes based dye sensitized solar cells: Fundamentals and research trends, Sol. Energy 207 (2020) 59–76, https://doi.org/10.1016/j.solener.2020.06.060.
[28] T.J. Castro, Using Grätzel cells as Arduino-controlled photosensors: proposals for the insertion of nanoscience and nanotechnology in classroom, Revista Brasileira De Ensino De Física 42 (2020), https://doi.org/10.1590/1806-9126-rbef-2020-0072.
[29] B. O'Regan, M. Grätzel, A low-cost, high-efficiency solar cell based on dye-sensitized colloidal TiO_2 films, Nature 353 (1991) 737–740, https://doi.org/10.1038/353737a0.
[30] A. Siddika, M. Sultana, M.S. Bashar, S. Tabassum, S. Aziz, M.A. Ali Shaikh, Improved performance of dye sensitized solar cell by exploration of photoanode and Ruthenium based dye, Opt Mater (Amst) 125 (2022) 112042. https://doi.org/10.1016/j.optmat.2022.112042.
[31] M. Younas, K. Harrabi, Performance enhancement of dye-sensitized solar cells via co-sensitization of ruthenium (II) based N749 dye and organic sensitizer RK1, Sol. Energy 203 (2020) 260–266, https://doi.org/10.1016/j.solener.2020.04.051.
[32] Md. SalauddinSk, R. Mia, M.A. Haque, A.M. Shamim, Review on Extraction and Application of Natural Dyes, Textile Leather Rev. (2021), https://doi.org/10.31881/TLR.2021.09.
[33] Amisse Ernestinho Dousane Milange, Evaluation of dyes for solar cells, Faculty of Science and Technology of the University of Coimbra, 2022.
[34] I.C. Carvalho, M.L. Barbosa, M.J.S. Costa, E. Longo, L.S. Cavalcante, V.G.F. Viana, R.S. Santos, TiO_2-based dye-sensitized solar cells prepared with bixin and norbixin

natural dyes: Effect of 2,2'-bipyridine additive on the current and voltage, Optik (Stuttg) 218 (2020), https://doi.org/10.1016/j.ijleo.2020.165236.
[35] E. Público Júnior, T. Nair Hojo Rebouças, A. Rebouças São José, I. Vilas Boas Souza, N. Oliveira Dias, Características de produção e teor de bixina em genótipos de urucueiros (Bixa orellana L.) em função da propagação, Revista Brasileira De Ciência, Tecnologia e Inovação 6 (2022) 69–77, https://doi.org/10.18554/rbcti.v6i2.5842.
[36] S.C. Alcázar-Alay, J.F. Osorio-Tobón, T. Forster-Carneiro, M.A.A. Meireles, Obtaining bixin from semi-defatted annatto seeds by a mechanical method and solvent extraction: Process integration and economic evaluation, Food Res. Int. 99 (2017) 393–402, https://doi.org/10.1016/j.foodres.2017.05.032.
[37] D. Raddatz-Mota, L.J. Pérez-Flores, F. Carrari, J.A. Mendoza-Espinoza, F.D. de León-Sánchez, L.L. Pinzón-López, G. Godoy-Hernández, F. Rivera-Cabrera, Achiote (Bixa orellana L.): a natural source of pigment and vitamin E, J. Food Sci. Technol. 54 (2017) 1729–1741, https://doi.org/10.1007/s13197-017-2579-7.
[38] E. Peksu, A. Coskun, H. Karaagac, Recent progress in solar cells based on one dimensional ZnO nanostructures, Nanotechnology 34 (2023) 352003, https://doi.org/10.1088/1361-6528/acda34.
[39] M.K. Otoufi, M. Ranjbar, A. Kermanpur, N. Taghavinia, M. Minbashi, M. Forouzandeh, F. Ebadi, Enhanced performance of planar perovskite solar cells using TiO_2/SnO_2 and TiO_2/WO_3 bilayer structures: Roles of the interfacial layers, Sol. Energy 208 (2020) 697–707, https://doi.org/10.1016/j.solener.2020.08.035.
[40] A.L.S. Resende, A.G.R. Costa, A.E.B. Lima, M.J.S. Costa, E. Longo, L.S. Cavalcante, R.S. Santos, An investigation of photovoltaic devices based on p-type Cu_2O and n-type γ-WO_3 junction through an electrolyte solution containing a redox pair, Int. J. Energy Res. 45 (2021) 2797–2809, https://doi.org/10.1002/ER.5974.
[41] K. Wu, Z. Wang, F. Nie, B. Ruan, H. Zhao, M. Wu, Pyrolysis synthesis of $CuWO_4$@C composite catalysts as Pt-free counter electrode for dye-sensitized solar cells, J. Anal. Appl. Pyrol. 170 (2023) 105873, https://doi.org/10.1016/j.jaap.2023.105873.
[42] D.B. Khadka, S. Sagadevan, S. Kato, T. Soga, Effect of annealing temperature on bismuth vanadate nano thin films for solar cell applications, Physica B Condens Matter 682 (2024) 415878, https://doi.org/10.1016/j.physb.2024.415878.
[43] G.S. Kamble, T.S. Natarajan, S.S. Patil, M. Thomas, R.K. Chougale, P.D. Sanadi, U. S. Siddharth, Y.-C. Ling, $BiVO_4$as a Sustainable and Emerging Photocatalyst: Synthesis Methodologies, Engineering Properties, and Its Volatile Organic Compounds Degradation Efficiency, Nanomaterials 13 (2023) 1528, https://doi.org/10.3390/nano13091528.
[44] J. Zhang, W. Luo, W. Li, X. Zhao, G. Xue, T. Yu, C. Zhang, M. Xiao, Z. Li, Z. Zou, A dye-free photoelectrochemical solar cell based on $BiVO_4$ with a long lifetime of photogenerated carriers, Electrochem. Commun. 22 (2012) 49–52, https://doi.org/10.1016/j.elecom.2012.05.027.
[45] D. Karthigaimuthu, P. Saradhi Maram, B. Arjun Kumar, G. Ramalingam, T. Elangovan, S. Sangaraju, Hydrothermal synthesis of MoS_2-$Mg(OH)_2$-$BiVO_4$ ternary hierarchical heterostructures for dye-sensitized solar cell application, Mater. Lett. 359 (2024) 135890, https://doi.org/10.1016/j.matlet.2024.135890.
[46] M. Mousavi-Kamazani, Cube-like Cu/Cu_2O/$BiVO_4$/Bi_7VO_{13} composite nanoparticles: Facile sol-gel synthesis for photocatalytic desulfurization of thiophene under visible light, J. Alloy. Compd. 823 (2020) 153786, https://doi.org/10.1016/j.jallcom.2020.153786.
[47] X. Li, M. Jia, Y. Lu, N. Li, Y.-Z. Zheng, X. Tao, M. Huang, $Co(OH)_2$/$BiVO_4$ photoanode in tandem with a carbon-based perovskite solar cell for solar-driven overall water splitting, Electrochim. Acta 330 (2020) 135183, https://doi.org/10.1016/j.electacta.2019.135183.
[48] S. Lotfi, M. El Ouardi, H.A. Ahsaine, A. Assani, Recent progress on the synthesis, morphology and photocatalytic dye degradation of $BiVO_4$ photocatalysts: A review, Catal. Rev. 66 (2024) 214–258, https://doi.org/10.1080/01614940.2022.2057044.
[49] Y.-S. Chen, J.S. Manser, P.V. Kamat, All Solution-Processed Lead Halide Perovskite-$BiVO_4$ Tandem Assembly for Photolytic Solar Fuels Production, J. Am. Chem. Soc. 137 (2015) 974–981, https://doi.org/10.1021/ja511739y.
[50] J. Ge, X. Ding, D. Jiang, L. Zhang, P. Du, Efficient Improved Charge Separation of FeP Decorated Worm-Like Nanoporous $BiVO_4$ Photoanodes for Solar-Driven Water Splitting, Catal. Lett. 151 (2021) 1231–1238, https://doi.org/10.1007/s10562-020-03398-3.
[51] Z. Zhang, X. Huang, Y. Bi, High-efficiency and stable syngas production by coupling NiFe-BiVO4 photoanodes with AgOx/Ag cathodes, Appl. Catal. B: Environ. Energy 349 (2024) 123894, https://doi.org/10.1016/j.apcatb.2024.123894.
[52] R. Packiaraj, K.S. Venkatesh, P. Devendran, S.A. Bahadur, N. Nallamuthu, Structural, morphological and electrochemical studies of nanostructured $BiVO_4$ for supercapacitor application, Mater. Sci. Semicond. Process. 115 (2020) 105122, https://doi.org/10.1016/j.mssp.2020.105122.
[53] I. Fuentes-Camargo, J.E. Carrera-Crespo, J. Vazquez-Arenas, I. Romero-Ibarra, J. L. Rodríguez, L. Lartundo-Rojas, J. Cardoso-Martínez, Pulse-Plating Electrodeposition of Metallic Bi in an Organic-Free Aqueous Electrolyte and Its Conversion into $BiVO_4$to Improve Photoelectrochemical Activity toward Pollutant Degradation under Visible Light, J. Phys. Chem. C 124 (2020) 1421–1428, https://doi.org/10.1021/acs.jpcc.9b09898.
[54] V.O. Smilyk, S.S. Fomanyuk, G.Y. Kolbasov, I.A. Rusetskyi, V.S. Vorobets, Electrodeposition, optical and photoelectrochemical properties of $BiVO_4$ and $BiVO_4$/WO_3 films, Res. Chem. Intermed. 45 (2019) 4149–4161, https://doi.org/10.1007/s11164-019-03897-y.
[55] L.P. Fontinele, R.C. de Sousa, V.G.F. Viana, E.A. de O. Farias, E.L. Queiroz, C. Eiras, Norbixin extracted from urucum (Bixa orellana L.) for the formation of conductive composites with potential applications in electrochemical sensors, Surf. Interfaces 13 (2018) 92–100, https://doi.org/10.1016/j.surfin.2018.08.002.
[56] Q.I. Zwane, S. Moeno, L.N. Dlamini, A multiphase $BiVO_4$ with the potential of being an environmental photocatalyst, Appl. Nanosci. 9 (2019) 539–555, https://doi.org/10.1007/s13204-018-0917-3.
[57] H. Saada, R. Abdallah, B. Fabre, D. Floner, S. Fryars, A. Vacher, V. Dorcet, C. Meriadec, S. Ababou-Girard, G. Loget, Boosting the Performance of $BiVO_4$ Prepared through Alkaline Electrodeposition with an Amorphous Fe Co-Catalyst, Chem. Electro Chem. 6 (2019) 613–617, https://doi.org/10.1002/celc.201801443.
[58] F. Zhan, J. Li, W. Li, Y. Liu, R. Xie, Y. Yang, Y. Li, Q. Chen, In situ formation of $CuWO_4$/WO_3 heterojunction plates array films with enhanced photoelectrochemical properties, Int. J. Hydrogen Energy 40 (2015) 6512–6520, https://doi.org/10.1016/j.ijhydene.2015.03.131.
[59] M. Zhao, X. Yan, L. Ren, M. Zhao, F. Guo, J. Zhuang, Y. Du, W. Hao, The role of oxygen vacancies in the high cycling endurance and quantum conductance in $BiVO_4$-based resistive switching memory, InfoMat 2 (2020) 960–967, https://doi.org/10.1002/inf2.12085.
[60] Q. Yuan, L. Chen, M. Xiong, J. He, S.-L. Luo, C.-T. Au, S.-F. Yin, Cu_2O/$BiVO_4$ heterostructures: synthesis and application in simultaneous photocatalytic oxidation of organic dyes and reduction of Cr(VI) under visible light, Chem. Eng. J. 255 (2014) 394–402, https://doi.org/10.1016/j.cej.2014.06.031.
[61] S.S. Patil, M.G. Mali, M.A. Hassan, D.R. Patil, S.S. Kolekar, S.-W. Ryu, One-Pot in Situ Hydrothermal Growth of $BiVO_4$/Ag/rGO Hybrid Architectures for Solar Water Splitting and Environmental Remediation, Sci. Rep. 7 (2017) 8404, https://doi.org/10.1038/s41598-017-08912-z.
[62] Z. Zhang, M. Wang, W. Cui, H. Sui, Synthesis and characterization of a core–shell $BiVO_4$ @g-C_3N_4 photo-catalyst with enhanced photocatalytic activity under visible light irradiation, RSC Adv. 7 (2017) 8167–8177, https://doi.org/10.1039/C6RA27766G.
[63] H.T.T. Nguyen, D. Jung, C.Y. Park, D.J. Kang, Synthesis of single-crystalline sodium vanadate nanowires based on chemical solution deposition method, Mater. Chem. Phys. 165 (2015) 19–24, https://doi.org/10.1016/J.MATCHEMPHYS.2015.05.053.
[64] L.E. Gomes, A.C. Nogueira, M.F. da Silva, L.F. Plaça, L.J.Q. Maia, R.V. Gonçalves, S. Ullah, S. Khan, H. Wender, Enhanced photocatalytic activity of $BiVO_4$/Pt/PtOx photocatalyst: The role of Pt oxidation state, Appl. Surf. Sci. 567 (2021) 150773, https://doi.org/10.1016/J.APSUSC.2021.150773.
[65] L.E. Gomes, L.F. Plaça, W.S. Rosa, R.V. Gonçalves, S. Ullah, H. Wender, Increasing the Photocatalytic Activity of $BiVO_4$ by Naked $Co(OH)_2$ Nanoparticle Cocatalysts, Photochem 2 (2022) 866–879, https://doi.org/10.3390/photochem2040055.
[66] J. Tauc, Optical properties and electronic structure of amorphous Ge and Si, Mater. Res. Bull. 3 (1968) 37–46, https://doi.org/10.1016/0025-5408(68)90023-8.
[67] B.D. Viezbicke, S. Patel, B.E. Davis, D.P. Birnie, Evaluation of the Tauc method for optical absorption edge determination: ZnO thin films as a model system, Physica Status Solidi (b) 252 (2015) 1700–1710, https://doi.org/10.1002/pssb.201552007.
[68] J. Wu, Z. Lan, J. Lin, M. Huang, Y. Huang, L. Fan, G. Luo, Electrolytes in Dye-Sensitized Solar Cells, Chem. Rev. 115 (2015) 2136–2173, https://doi.org/10.1021/cr400675m.
[69] F. Bella, S. Galliano, M. Falco, G. Viscardi, C. Barolo, M. Grätzel, C. Gerbaldi, Unveiling iodine-based electrolytes chemistry in aqueous dye-sensitized solar cells, Chem. Sci. 7 (2016) 4880–4890, https://doi.org/10.1039/C6SC01145D.
[70] M.A.K.L. Dissanayake, K. Umair, G.K.R. Senadeera, J.M.K.W. Kumari, Effect of electrolyte conductivity, co-additives and mixed cation iodide salts on efficiency enhancement in dye sensitized solar cells with acetonitrile-free electrolyte, J. Photochem. Photobiol. Chem. 415 (2021) 113308, https://doi.org/10.1016/j.jphotochem.2021.113308.
[71] M.M. Varishetty, M. Kenji, N. Tarannum, S.R. Damaraju, M. Jonnalagadda, A novel poly(acrylonitrile)/poly(ethylene glycol)-based polymer gel electrolyte for high efficiency dye sensitized solar cells, Energy Adv. 2 (2023) 1702–1712, https://doi.org/10.1039/D3YA00079F.
[72] A.E.B. Lima, M.J.S. Costa, R.S. Santos, N.C. Batista, L.S. Cavalcante, E. Longo, G. E. Luz, Facile preparation of $CuWO_4$ porous films and their photoelectrochemical properties, Electrochim. Acta 256 (2017) 139–145, https://doi.org/10.1016/j.electacta.2017.10.010.
[73] J.E. Yourey, B.M. Bartlett, Electrochemical deposition and photoelectrochemistry of $CuWO_4$, a promising photoanode for water oxidation, J. Mater. Chem. 21 (2011) 7651, https://doi.org/10.1039/c1jm11259g.
[74] W. Yang, R.R. Prabhakar, J. Tan, S.D. Tilley, J. Moon, Strategies for enhancing the photocurrent, photovoltage, and stability of photoelectrodes for photoelectrochemical water splitting, Chem. Soc. Rev. 48 (2019) 4979–5015, https://doi.org/10.1039/C8CS00997J.
[75] A. Hankin, F.E. Bedoya-Lora, J.C. Alexander, A. Regoutz, G.H. Kelsall, Flat band potential determination: avoiding the pitfalls, J. Mater. Chem. A Mater. 7 (2019) 26162–26176, https://doi.org/10.1039/C9TA09569A.
[76] A.E.B. Lima, M. Assis, A.L.S. Resende, H.L.S. Santos, L.H. Mascaro, E. Longo, R. S. Santos, L.S. Cavalcante, G.E. Luz, $CuWO_4$|$MnWO_4$ heterojunction thin film with improved photoelectrochemical and photocatalytic properties using simulated

solar irradiation, Journal of Solid-State, Electrochemistry 26 (2022) 997–1011, https://doi.org/10.1007/s10008-022-05143-9.

[77] M.J.S. Costa, G.S. Costa, L.G.P. Morais, A.G.R. Costa, E.P. Ribeiro, R.M.P. Silva, G. E. Luz Jr, R.S. Santos, Progesterone photoelectrocatalytic degradation on $NiWO_4$| $CoWO_4$ homojunction film, Catal. Today 442 (2024) 114955, https://doi.org/10.1016/j.cattod.2024.114955.

[78] S. Daemi, S. Kaushik, S. Das, T.W. Hamann, F.E. Osterloh, $BiVO_4$–Liquid Junction Photovoltaic Cell with 0.2% Solar Energy Conversion Efficiency, J. Am. Chem. Soc. 145 (2023) 25797–25805, https://doi.org/10.1021/jacs.3c09546.